DOI: 10.1002/ejic.201000608

TiO_2 Nanotubes – Annealing Effects on Detailed Morphology and Structure

Sergiu P. Albu,[a] Hiroaki Tsuchiya,[b] Shinji Fujimoto,[b] and Patrik Schmuki*[a]

Keywords: Titanium / Nanotubes / Crystallization / Anodization / DSSC / Electrochemistry

The present work deals with self-organized TiO_2 nanotube layers formed on a Ti metal substrate by anodization. For virtually any electrical or photoelectric application, these originally amorphous nanotube layers need to be converted to anatase. Most frequently, this is done by annealing at temperatures of approximately 450 °C. In the present work we use TEM and XRD to compare the annealing at a significantly lower temperature of 350 °C with that at the established 450 °C. HRTEM results show that both annealing treatments lead to comparable grain sizes in the nanotube walls; however, at 450 °C numerous defects (nanoscopic cracks) are created in the nanotube walls. Moreover, the treatment at 450 °C leads to the formation of a (rutile) oxide layer underneath the tube layers. These factors can considerably affect the overall properties of the tubes. Additionally, we point out some effects that should be carefully considered when using HRTEM investigation on TiO_2 nanotubes such as e-beam-induced crystallization or tube diameter shrinkage.

Introduction

In the last decade, TiO_2 nanotube layers have attracted considerable interest for various scientific and technological reasons. After the first report by Zwilling[1] on the self-organized formation of TiO_2 nanotubes by electrochemical anodization of Ti metal in a fluoride-containing solution, the morphology, in particular, the tube-wall smoothness, aspect ratio, and diameter control were increasingly improved.[2] The TiO_2 nanotube layers have a high number of potential applications based on their ion insertion,[3] electronic or biomedical properties[4] (for an overview see ref.[5]). After electrochemical formation, the oxide tubes are amorphous, but for many applications the conversion to an anatase crystal structure is desired. Typically annealing the TiO_2 tubes in air at temperatures greater than 300 °C alters them to an anatase structure,[6] whereas at temperatures greater than 500 °C, an increasing amount of rutile is formed.[6e,7] The anatase phase is beneficial for biomedical applications,[4b] but full conversion to anatase is even more significant in photoelectric applications such as photocatalysis and other applications that critically depend on a high electron-transport efficiency along the tube walls. Most recently, it was reported that for TiO_2 nanotube layers used in Grätzel type dye-sensitized solar cells, electron mobilities[8] and electron diffusion lengths can be measured[9] that are considerably higher than those in conventional particle-based cells.[9b] First results showed that the electron transport times can be drastically affected by the annealing conditions.[10] In fact, an up to 10× higher electron mobility was reported for TiO_2 nanotubes used in Grätzel type solar cells that were constructed with tubes annealed at 350 °C rather than at 450 °C. Furthermore, this different behavior is very significant as by far the most frequently used annealing temperature for TiO_2 nanotubes is approximately 400–450 °C.[6d,11] The present work provides investigations of structural and morphological effects that occur at different annealing temperatures.

Results and Discussion

TiO_2 nanotube layers were formed by anodization of a Ti sheet in a fluoride-containing ethylene glycol electrolyte as described in the Experimental Section. Figure 1a shows a SEM cross-sectional view of the resulting TiO_2 nanotube arrays. The tube length was reproducibly established at 25 μm, and the outer tube diameter was about 160 nm. Figure 1b shows XRD spectra taken for the as-formed tubes and for tubes annealed in air at 350 and 450 °C. The XRD results show that annealing at both temperatures converts the originally amorphous tubes entirely to anatase. The annealed TiO_2 nanotubes show peak intensity characteristics similar to the diffraction patterns for anatase powder with the highest peak in the (101) direction. Thus, one may suppose that there is no preferential orientation of crystallites inside the tubes (Figure 1b).

Figures 1c and d show TEM images of tubes annealed at 350 and 450 °C, respectively. From the images, one can deduce that the wall thickness of the tubes with 160 nm diameter is approximately 40 nm. The diffraction patterns in Figures 1e and f confirm that the tube walls consist of anatase TiO_2. During measurements, we observed in diffraction

[a] Department of Materials Science, Institute for Surface Science and Corrosion (LKO), University of Erlangen-Nuremberg, Martensstrasse 7, 91058 Germany
Fax: +49-9131-852-7582
E-mail: schmuki@ww.uni-erlangen.de
[b] Division of Materials and Manufacturing Science, Graduate School of Engineering, Osaka University, 2-1 Yamada-oka, Suita, Osaka 565-0871 Japan

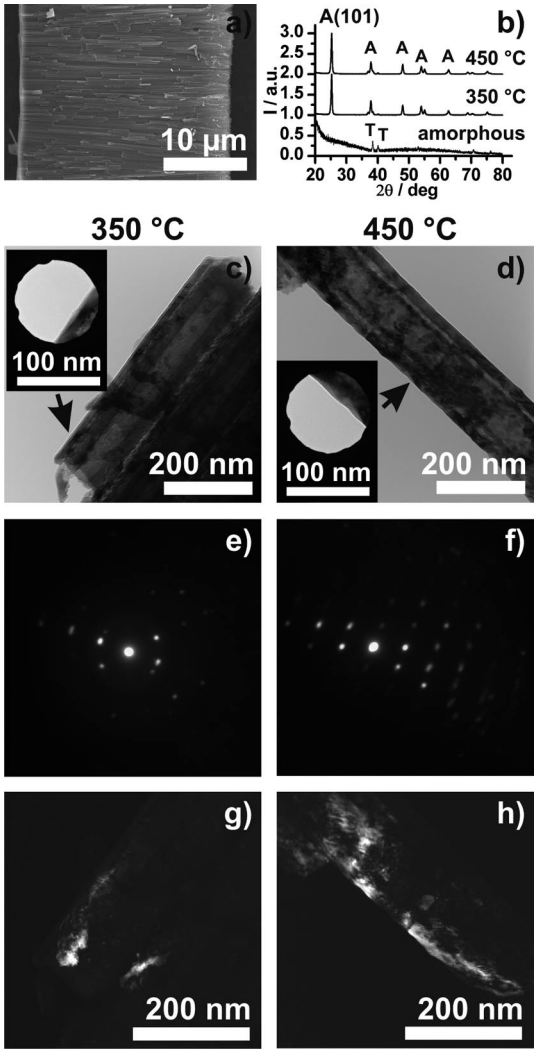

Figure 1. (a) SEM cross-section of as-formed TiO_2 nanotubes. (b) XRD of the samples. (c, d) TEM images of the samples annealed at 350 and 450 °C. Insets represent selected areas. (e, f) Diffraction pattern obtained from the chosen selected areas. (g, h) Dark-field images of the TiO_2 nanotubes. (In XRD the peaks marked A represent anatase and those marked T show titanium [metal]).

patterns taken from entire nanotubes that some orientations give higher intensities, which indicated that the signal is composed of contributions of considerably large crystals and smaller crystallites. The dark-field images displayed in Figures 1g and h, taken for a specific orientation from the diffraction patterns, show the size of the analyzed crystal. These are typical crystallites with lengths of about 1 µm and diameters of approximately 160 nm. This means that the crystals in the nanotube walls at 350 and 450 °C are of similar size. Figure 2 shows a HRTEM image taken from the top of a tube ring. It indicates that the crystals are of cylindrical shape. In other words, under both annealing conditions the tube wall mainly consists of crystals of comparable size with a cylindrical shape that can be several hundred nanometers long in the direction of the nanotube axis.

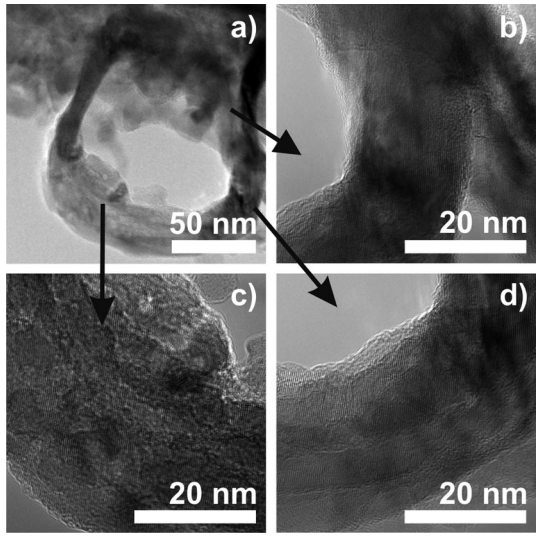

Figure 2. (a, b, c, d) HRTEM images of a tube top showing a single crystal with a cylindrical shape.

However, more detailed TEM and SEM investigations as shown in Figure 3 reveal considerable differences in the nanotube walls for the different annealing temperatures. The samples annealed at 450 °C show in the SEM some dark line patterns on the tube walls, whereas this pattern is absent at 350 °C. These lines are, as we will show below, interfaces/borders between crystallites. A closer look at the interfaces between crystals by using HRTEM shows that numerous cracks are present in samples annealed at 450 °C. Figure 3c shows a HRTEM image of the sample annealed at 350 °C with a generally smooth surface and a continuous lattice structure across grain boundaries. In contrast, for samples annealed at 450 °C quite large cracks are present at many grain boundaries, and a high number of them can be found along the nanotubes (Figure 3d). The appearance of cracks and their increased density at higher crystallization temperatures may be ascribed to larger stress occurring during crystallization, heating, and cooling.

One might assume that the cracks occurring at an annealing temperature of 450 °C could be avoided by slower ramping speeds. However, even at slow temperature-rise rates such as 0.1 °C/s, one can still observe the crack morphology as shown in Figure 3f. Furthermore, the findings presented here (cracks) are not limited to the specific fabrication conditions of the nanotubes used in this work but can be observed for a wide range of growth conditions.

Another important effect of the annealing temperature is shown in Figure 4. If the region at bottom of the tube is inspected closely with FE-SEM (cross-sections shown in Figures 4a, b), one can see that an additional oxide layer is present underneath the tubes, that is, the annealing treatment causes not only a conversion of amorphous tubes to anatase TiO_2 but also some direct thermal oxidation of the metal substrate underneath. It can be seen that, at 350 °C, the layer is approximately 50 nm thick, while at 450 °C, the thickness is approximately 140 nm. For comparison, we also annealed a plain Ti substrate under the same condi-

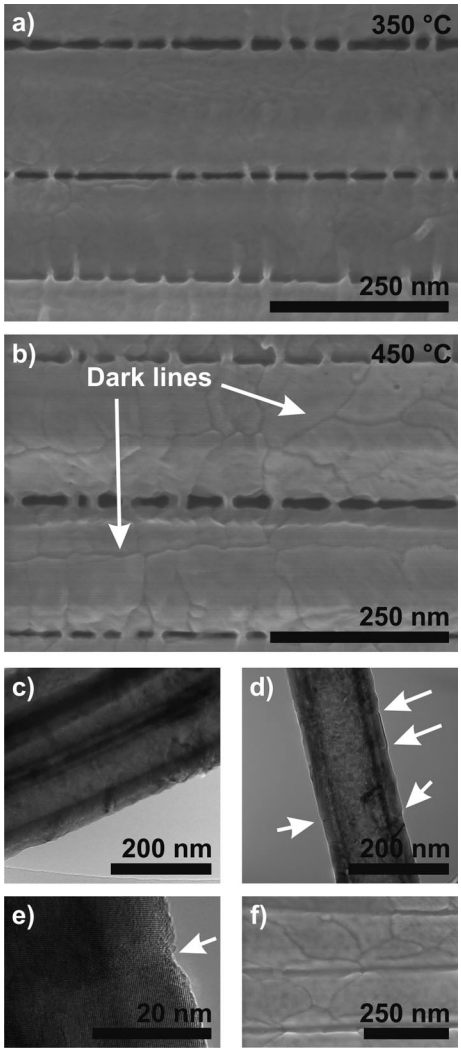

Figure 3. (a, b) High-magnification SEM cross-section of nanotubes annealed at 350 and 450 °C. (c) HRTEM image of nanotubes annealed at 350 °C. (d) HRTEM image of tubes annealed at 450 °C. Arrows indicate the sites where a crack is formed; (e) HRTEM image of a tube wall annealed at 450 °C showing the interface of the crystals (see arrow); (f) High-magnification SEM cross-section of nanotubes annealed at 450 °C with a lower temperature-rise rate of 0.1 °C/s.

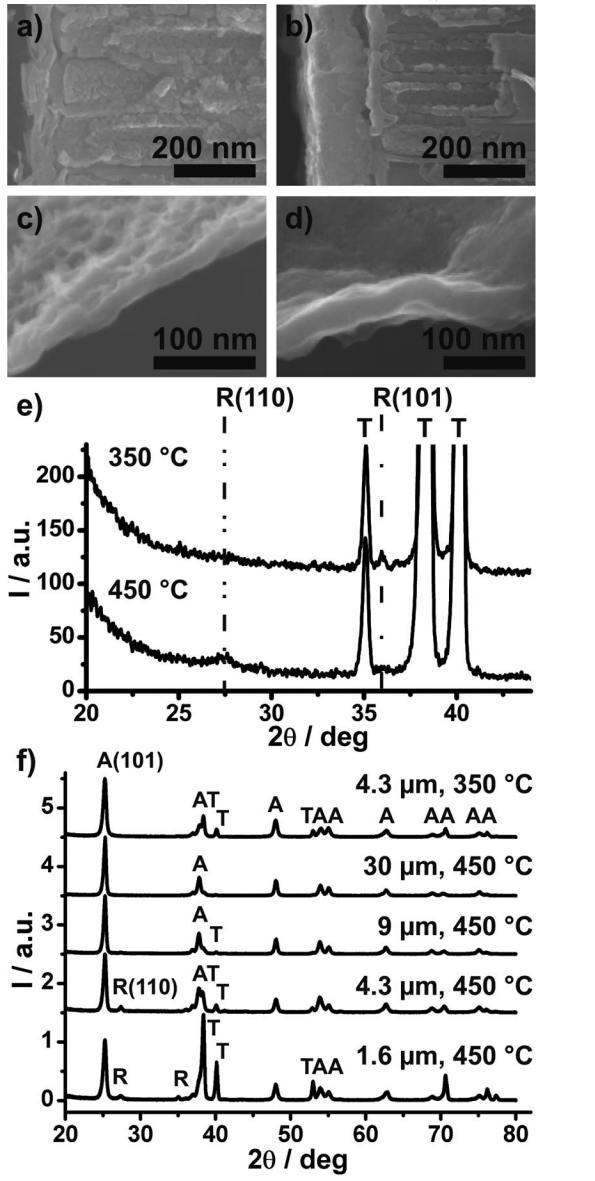

Figure 4. (a, b) HRSEM cross-sectional view near the bottoms of the TiO_2 nanotubes at 350 and 450 °C; (c, d) thickness of the rutile layer formed on top of pure Ti at 350 and 450 °C. (e) XRD of the oxides grown at 350 and 450 °C on pure titanium; (f) XRD of the TiO_2 nanotube arrays of different thicknesses. (In XRD the peaks marked A represent anatase, those marked R stand for rutile, and those marked T show titanium [metal]).

tions and obtained the thermal oxide layers shown in Figures 4c, d.

These layers were found to have a thickness of 20 nm for 350 °C and 50 nm for 450 °C. This thickness is well in line with literature results for thermal oxidation of Ti in air.[12] By comparison (the results are compiled in Table 1), the oxide layer is much thicker underneath the tubes than the oxide layer formed on a pure titanium surface under the same annealing conditions.

It should be pointed out, however, that the bottom layer underneath the tubes typically contains a fluoride-rich layer,[6e,13] that is, a different chemical environment is present, which may be responsible for the thicker oxide layer formation observed for tubes. Figure 4e shows the XRD analysis of the reference thermal oxides formed on the surface of pure titanium. It can be seen that the oxide grown at 350 °C has a weak peak of rutile at $2\theta = 36.09°$, which corresponds to the (101) plane orientation. This peak has only 50% of the intensity of the same peak in an XRD spectrum of rutile powder.[14] This suggests that the rutile crystal nucleation

Table 1. Layer thicknesses grown underneath TiO_2 nanotubular layers and those grown on pure Ti surfaces.

	Thickness of TiO_2 grown	
Thermal conditions	on a pure Ti surface	underneath tubes
350 °C, 3 h, 1 °C/s	ca. 20 nm (rutile)	ca. 50 nm (rutile)
450 °C, 3 h, 1 °C/s	ca. 50 nm (rutile)	ca. 140 nm (rutile)

has a preferential orientation in the layer. In the case of the 450 °C sample, the amount of rutile increases, and the main (110) peak appears as the most intense of all three peaks of rutile detectable in this layer [2θ = 27.45° (110), 2θ = 36.09° (101), and 2θ = 54.32° (211)]. The formation of rutile by thermal oxidation of metallic Ti is quite commonly observed.[15] For the TiO_2 nanotube layers, one can show that at 350 and 450 °C only the newly formed thermal oxide consists of rutile, whereas the tube wall (converted from amorphous material) consists fully of anatase. This is not only supported by the TEM investigations in Figure 3 but also by XRD spectra taken from different tube layer thicknesses (Figure 4f).

The preparation of these different tube lengths is described in the Experimental Section. For thin tubular layers, the XRD spectra contain information on the whole layer, that is, the penetration depth is sufficient to include the thermal oxide at the interface and the titanium substrate. Under the present XRD analysis conditions, the X-ray penetration depth is approximately 9 μm.[16] At higher thicknesses, the TiO_2 nanotube layer is not anymore fully penetrated and therefore only contains information on the tube walls. Accordingly, a decrease in the rutile peak intensity is observed for thicker layers. For the 30 μm thick layers, the rutile peaks are completely absent. Evaluated data are compiled in Table 2.

Table 2. Intensity of the main rutile peak.

Thickness	1.6 μm	4.3 μm	9 μm	30 μm
I_R (110)	3.3	3.2	1.8	0

These results are a critical finding regarding the annealing of TiO_2 nanotubes, as a substantial part of literature reports that rutile is formed in the tubes at temperatures as low as 430 °C.[17] Clearly, the findings of the present work are in conflict with such statements.

Some interesting side aspects emerged during structural investigations of the TiO_2 nanotubes by using HRTEM. Namely, it was evident already after some few experiments that significant changes in the structure and morphology of amorphous nanotubes can be induced by e-beam irradiation. As previously observed,[18] TiO_2 is prone to e-beam-induced crystallization, as illustrated in Figure 5. Figures 5a and b show the HRTEM images of amorphous TiO_2 nanotubes that were taken before and after e-beam exposure for several minutes at 200 kV. Clearly, the formation of crystalline zones can be seen (lattice fringes appear) with increasing TEM observation time. The amount and size of these crystallites increase in time. Moreover, crystallization is accompanied by a shrinkage effect of the TiO_2 nanotubes, as shown in Figure 6. Figures 6a, b show a tube bottom range before and after TEM observations for some time, and Figures 6c, d show a tube wall location before and after TEM observation. Both images show that crystallization leads to considerable volume contraction and therefore a deformation of the nanotube geometry. In the case of Figure 6d, after exposure of about 10 min, one side of the tube suf-

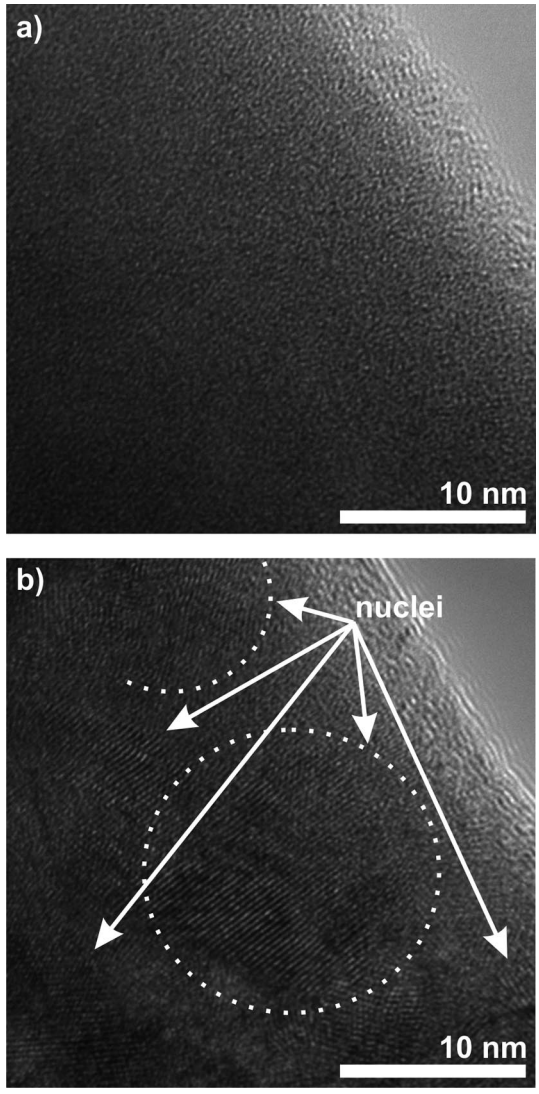

Figure 5. HRTEM images of amorphous TiO_2 nanotubes before (a) and after (b) e-beam exposure for several minutes at 200 kV.

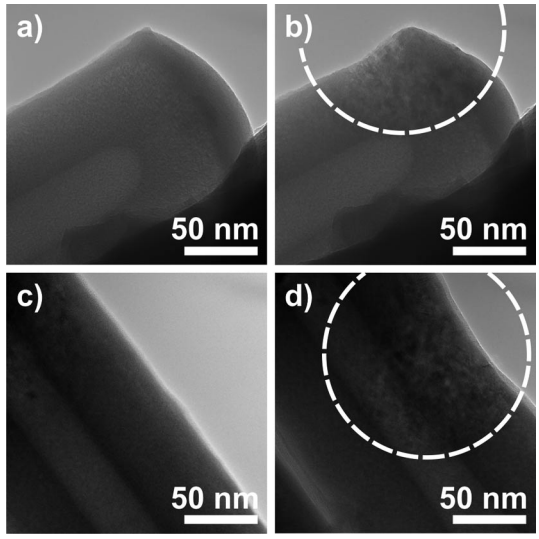

Figure 6. (a, b) Shrinkage effect of the amorphous nanotubes at the tube bottom under exposure to the TEM e-beam for about 12 min; (c, d) shrinkage effect of the amorphous nanotubes under exposure to the TEM e-beam for about 10 min.

fered a lateral shrinkage of about 15 nm. The exposed area is filled with arbitrary oriented crystallites with sizes of approximately 25 nm.

Conclusions

The present work shows that annealing of anodic TiO_2 nanotubes at two different temperatures (both frequently used to crystallize the nanotubes to anatase) can induce some significant differences in the detailed tube structure. While the crystallite size in the tube walls is approximately the same for both temperatures, HRTEM reveals a significant amount of cracks in the tube wall when annealing is performed at 450 °C. Moreover, annealing in air leads to a comparably thick rutile layer at the metal/tube bottom interface (due to thermal oxidation of the substrate). Both effects (cracks and rutile layer) are a plausible origin of the significantly slower electron transport times observed for tubes annealed at 450 °C, as reported in literature.[9a,19] On the one hand, the cracks represent obstacles for electron transport and thus may lead to larger effective diffusion lengths (around the crack). On the other hand, the formation of rutile layers may affect the electron transport in solar cells to the back contact (Ti substrate), as rutile has a significantly lower electron mobility than anatase.[20] At the present stage, it is not clear whether observed cracks or rutile layers can be avoided by an optimization of the annealing treatment at higher temperatures. For solar cells, annealing at higher temperature is desired, as it has been observed that for dye-sensitized solar cells (DSSCs) the areal loading of dye is improved for tubes annealed at higher temperatures.[10]

When investigating amorphous TiO_2 nanotubes by HRTEM experiments, we found some significant e-beam-induced crystallization effects, which, in turn, also affect the overall tube morphology. In other words, HRTEM work reporting the presence of crystallites in as-formed TiO_2 nanotubes (without additional proof) has to be examined very carefully.

Experimental Section

As substrates for TiO_2 nanotube growth, we used titanium foil (99.6% purity, Goodfellow) with a thickness of 0.1 mm. Prior to tube formation, the foils were cleaned by sonication in acetone and ethanol followed by rinsing with deionized water and drying in a nitrogen stream. To perform the electrochemical TiO_2 nanotube formation, the foils were anodized by using a high-voltage potentiostat (Jaissle IMP 88 PC) in a two-electrode configuration with a counterelectrode made of platinum gauze. The electrolyte was a fresh solution of ethylene glycol (Riedel-de Haën, 24204) with addition of HF (0.5 M, 40%, Merck) and deionized H_2O (1 M). Anodization was carried out at 100 V, and layers of 25 μm thickness were grown by passing a charge density of 45 C/cm^2. Other tube lengths were obtained under the same conditions by varying the anodization time to reach a specific charge density (1.6 μm, 3 C/cm^2; 4.3 μm, 7.7 C/cm^2; 9 μm, 16 C/cm^2; 30 μm, 54 C/cm^2;). After the experiment, the samples were immersed in ethanol for 1 h and then dried in an N_2 stream. All experiments were carried out at a temperature of 20 °C. Samples were annealed at two different temperatures (350 and 450 °C) for 3 h in air with a temperature-rise rate of 1 °C/s by using a Rapid Thermal Annealer – Jipelec JetFirst 100. To investigate the influence of the annealing rate, some experiments were performed at 0.1 °C/s. The complete thickness of this layer was obtained by dissolution of the Ti substrate with a very highly selective anhydrous methanol/Br_2 (9:1 vol) solution. This solution dissolves titanium, but not titanium dioxide. A field-emission scanning electron microscope (Hitachi FE-SEM S4800) and transmission electron microscope (Hitachi TEM H-800 and HF-2000) were used for morphological characterization of the samples. The length of the nanotubes was measured from SEM cross-sections. X-ray diffraction analysis (XRD) was performed with a Xpert Philips PMD having a Panalytical Xcelerator detector using graphite-monochromatized Cu-K_α radiation. The incident X-ray beam impinged on the sample at an angle of 5° and stayed fixed during the measurement in a 2θ scan mode.

Acknowledgments

The present work is partially supported by the "Priority Assistance of the Formation of Worldwide Renowned Centers of Research – Global COE Program (Project: Center of Excellence for Advanced Structural and Functional Materials Design)" and the Grant-in-Aid (Project N. 20760493) from the Ministry of Education, Culture, Sports, Science and Technology of Japan. A part of the present work was carried out by using a facility in the Research Center for Ultra High Voltage Electron Microscopy, Osaka University. Additionally we acknowledge financial support by Deutsche Forschungsgemeinschaft (DFG) [Engineering of Advanced Materials (EAM) (catalysis section) Cluster of Excellence] and other DFG grants.

[1] V. Zwilling, E. Darque-Ceretti, A. Boutry-Forveille, D. David, M. Y. Perrin, M. Aucouturier, *Surf. Interface Anal.* **1999**, *27*, 629–637.

[2] a) J. M. Macak, K. Sirotna, P. Schmuki, *Electrochim. Acta* **2005**, *50*, 3679–3684; b) J. M. Macak, H. Tsuchiya, P. Schmuki, *Angew. Chem. Int. Ed.* **2005**, *44*, 2100–2102; c) J. M. Macak, H. Tsuchiya, L. Taveira, S. Aldabergerova, P. Schmuki, *Angew. Chem. Int. Ed.* **2005**, *44*, 7463–7465; d) S. Bauer, S. Kleber, P. Schmuki, *Electrochem. Commun.* **2006**, *8*, 1321–1325.

[3] a) R. Hahn, A. Ghicov, H. Tsuchiya, J. M. Macak, A. G. Munoz, P. Schmuki, *Phys. Status Solidi A* **2007**, *204*, 1281–1285; b) A. Ghicov, H. Tsuchiya, R. Hahn, J. M. Macak, A. G. Munoz, P. Schmuki, *Electrochem. Commun.* **2006**, *8*, 528–532; c) C. L. Olson, J. Nelson, M. S. Islam, *J. Phys. Chem. B* **2006**, *110*, 9995–10001.

[4] a) Y.-T. Sul, B. Johansson Carina, S. Petronis, A. Krozer, Y. Jeong, A. Wennerberg, T. Albrektsson, *Biomaterials* **2002**, *23*, 491–501; b) D. M. Brunette, P. Tengvall, M. Textor, P. Thomsen, (Editors), *Titanium in Medicine*, Springer, Berlin, **2001**.

[5] a) J. M. Macak, H. Tsuchiya, A. Ghicov, K. Yasuda, R. Hahn, S. Bauer, P. Schmuki, *Curr. Opin. Solid State Mater. Sci.* **2007**, *11*, 3–18; b) A. Ghicov, P. Schmuki, *Chem. Commun.* **2009**, 2791–2808.

[6] a) R. Beranek, H. Tsuchiya, T. Sugishima, J. M. Macak, L. Taveira, S. Fujimoto, H. Kisch, P. Schmuki, *Appl. Phys. Lett.* **2005**, *87*, 243114–243116; b) A. Ghicov, J. M. Macak, H. Tsuchiya, J. Kunze, V. Haeublein, L. Frey, P. Schmuki, *Nano Lett.* **2006**, *6*, 1080–1082; c) A. Ghicov, H. Tsuchiya, J. M. Macak, P. Schmuki, *Phys. Status Solidi A* **2006**, *203*, R28–R30; d) J. M. Macak, S. Aldabergerova, A. Ghicov, P. Schmuki, *Phys. Status Solidi A* **2006**, *203*, R67–R69; e) S. P. Albu, A. Ghicov, S. Alda-

bergenova, P. Drechsel, D. LeClere, G. E. Thompson, J. M. Macak, P. Schmuki, *Adv. Mater.* **2008**, *20*, 4135–4139.
[7] A. W. Czanderna, C. N. R. Rao, J. M. Honig, *Trans. Faraday Soc.* **1958**, *54*, 1069–1073.
[8] K. Zhu, N. R. Neale, A. Miedaner, A. J. Frank, *Nano Lett.* **2006**, *7*, 69–74.
[9] a) J. R. Jennings, A. Ghicov, L. M. Peter, P. Schmuki, A. B. Walker, *J. Am. Chem. Soc.* **2008**, *130*, 13364–13372; b) P. Roy, D. Kim, K. Lee, E. Spiecker, P. Schmuki, *Nanoscale* **2010**, *2*, 45–59.
[10] A. Ghicov, S. P. Albu, R. Hahn, D. Kim, T. Stergiopoulos, J. Kunze, C. A. Schiller, P. Falaras, P. Schmuki, *Chem. Asian J.* **2009**, *4*, 520–525.
[11] a) T. Stergiopoulos, A. Ghicov, V. Likodimos, D. S. Tsoukleris, J. Kunze, P. Schmuki, P. Falaras, *Nanotechnology* **2008**, *19*, 235602; b) S. C. Han, J. M. Doh, J. K. Yoon, G. H. Kim, J. Y. Byun, S. H. Han, K. T. Hong, S. I. Kwun, *Met. Mater. Int.* **2009**, *15*, 493–499.
[12] E. Gaul, *J. Chem. Educ.* **1993**, *70*, 176–178.
[13] P. Roy, S. Berger, P. Schmuki, *Angew. Chem. Int. Ed.* **2010**, accepted, DOI: 10.1002/anie.201001374.
[14] H. E. Swanson, H. F. McMurdie, M. C. Morris, E. H. Evans, *J. Res. Nat. Bur. Stand. Monogr.* **1969**, *7*, 1–188.
[15] a) E. Gemelli, N. H. A. Camargo, *Matéria (Rio de Janeiro)* **2007**, *12*, 525–531; b) J. W. Hickman, E. A. Gulbransen, *Anal. Chem.* **1948**, *20*, 158–165; c) C.-C. Ting, S.-Y. Chen, D.-M. Liu, *J. Appl. Phys.* **2000**, *88*, 4628–4633; d) R. D. Shannon, J. A. Pask, *Am. Mineral.* **1964**, *49*, 1707–1717.
[16] a) B. D. Cullity, *Elements of X-ray Diffraction*, Addison-Wesley, Massachusetts, **1956**, pp. 269–272; b) R. Guinebretière, *X-ray Diffraction by Polycrystalline Materials*, ISTE Ltd, London, **2007**, pp. 111–115; c) E. Prince (Ed.), *International Tables for Crystallography, Volume C: Mathematical, Physical and Chemical Tables* Kluwer Academic Publishers, Dordrecht, **2004**, pp. 230–231.
[17] O. K. Varghese, D. Gong, M. Paulose, C. A. Grimes, E. C. Dickey, *J. Mater. Res.* **2003**, *18*, 156–165.
[18] A. Aladjem, D. G. Brandon, J. Yahalom, J. Zahavi, *Electrochim. Acta* **1970**, *15*, 663–671.
[19] a) M. Gratzel, *Inorg. Chem.* **2005**, *44*, 6841–6851; b) H. J. Snaith, L. Schmidt-Mende, *Adv. Mater.* **2007**, *19*, 3187–3200.
[20] H. Tang, K. Prasad, R. Sanilines, P. E. Schmid, F. Levy, *J. Appl. Phys.* **1994**, *75*, 2042–2047.

Received: May 31, 2010
Published Online: August 16, 2010

